Received: 16 January 2021 | Revised: 3 March 2021 | Accepted: 3 March 2021

DOI: 10.1002/pol.20210030

ORIGINAL ARTICLE

JOURNAL OF POLYMER SCIENCE WILEY

Deformation and failure kinetics of polyvinylidene fluoride: Influence of crystallinity

Tommaso Pini[1] | **Martin van Drongelen**[2] | **Joris J. C. Remmers**[1] | **Marc G. D. Geers**[1] | **Leon E. Govaert**[1,2]

[1]Department of Mechanical Engineering, Eindhoven University of Technology, Eindhoven, The Netherlands

[2]Faculty of Engineering Technology, Chair of Production Technology, University of Twente, Enschede, The Netherlands

Correspondence
Tommaso Pini, Department of Mechanical Engineering, Eindhoven University of Technology, P.O. Box 513, 5600 MB, Eindhoven, The Netherlands.
Email: t.pini@tue.nl

Abstract

The present study investigates the effect of processing conditions on the yield kinetics, such as rate dependence of the yield stress and creep rupture, of polyvinilidene fluoride. Samples were compression molded with cooling rates varying from 100°C/s to 0.5°C/min, or isothermally crystallized at temperatures varying from 20 to 120°C. Deformation kinetics were studied over a wide range of strain rates and temperatures. It is shown that for all conditions the yield response is well represented by the Ree–Eyring model. Moreover, the activation volumes and activation energies are independent from the processing conditions. The effect of processing is fully covered by a simple relationship between the rate factors and the degree of crystallinity. Subsequently, the versatility of this relationship is demonstrated by experimental validation.

KEYWORDS

crystallinity, fluoropolymers, processing, PVDF, structure–property, yield, yield kinetics

1 | INTRODUCTION

Polyvinilidene fluoride (PVDF) is a semi-crystalline polymer with excellent gas barrier properties and high chemical resistance; apart from that, it is best known for its polymorphism. Five different crystalline phases can be found[1,2] but the α and β phases are the most common and frequently investigated ones. Generally, when the material is undercooled from the melt in quiescent conditions, a combination of α (TG^+TG^-) and mesomorphic phases is obtained, with an increase of the former with decreasing cooling rates. The β (TTT) phase, which is known for its piezo- and pyroelectrical properties, can be obtained by stretching from the α conformation[3–6]; however, the properties characterizing β-PVDF are not the subject of the present work. In this article, we focus on the mechanical properties of α-PVDF.

The mechanical properties of the material are related to the details of the microstructure: for example, the phase content, degree of crystallinity, and size of the crystalline domains. The morphology, in turn, is affected by the processing conditions in terms of cooling rate, flow, and pressure and it evolves in time depending on the thermo-mechanical history.[7–10]

Regardless the effect of processing, the good mechanical properties and the chemical resistance of PVDF drew great interest from industry, in particular for oil and gas field applications,[11,12] where a good performance of the material on a long-term time scale is fundamental. Since the adoption of polymeric pipes in the late 1950s, research on these materials focused on the understanding of the long-term mechanical performance. It is now well established that there are three failure mechanisms coexist

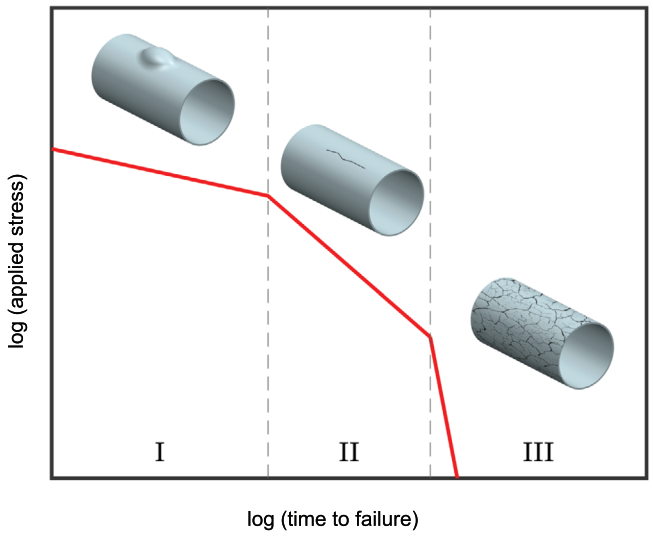

FIGURE 1 Sketch of the three regions of typical failure mechanisms for polymers [Color figure can be viewed at wileyonlinelibrary.com]

in polymers[13–16]; these mechanisms act in parallel but, depending on loading conditions, one of these may trigger catastrophic failure before the others. This results in three distinct regions typically observable in an applied stress-time to failure plot, as shown in the example of Figure 1:

1. Region I: plasticity-controlled failure, also referred as ductile failure. In this case failure is triggered by the accumulation of plastic deformation beyond a critical value. In most cases, failure is accompanied by large plastic deformation such as bulging.
2. Region II: slow crack growth, also referred as brittle failure. Existing defects grow under the action of the applied load up to a critical size leading to unstable propagation or loss of functionality (e.g., leaking if the defect grows through the thickness of a pipe).
3. Region III: molecular degradation. This process is essentially stress independent; moreover, it can be easily avoided (or shifted toward very long times) by the addition of stabilizers. Therefore, it is no longer considered a limiting factor for the long-term performance of polymeric pipes.

Compared to other thermoplastics, the long-term failure of PVDF received relatively limited attention; the crack growth kinetics were reported by Al-Abduljabbar et al.[17] who used an indirect technique based on fatigue tests on unnotched pipe segments. De Jesus Silva et al.[18] investigated and modeled the thermal degradation of PVDF aged in bioethanol.

With respect to creep rupture (plasticity-controlled failure), no studies were reported so far. This failure mode is closely related to the yield stress, which for PVDF is known to depend strongly on temperature and strain rate. The deformation kinetics of PVDF were studied extensively by Hellinckx and Bauwens,[19] who identified three separate molecular deformation mechanisms contributing to the yield stress in different conditions of temperature and strain rate. This response was successfully modeled using a Ree–Eyring approach.

Previously, Bauwens-Crowet et al.[20] already demonstrated that the stress dependence of the plastic flow rate during secondary creep is identical to $\sigma_y(\dot{\varepsilon})$ and showed that it can be employed to predict time to failure. This approach was later adopted by Kanters et al.[16] who developed it into a framework to predict time to failure in the plasticity-controlled failure of HDPE.

In the present investigation, this approach, which was proven successful also for other semi-crystalline polymers,[16,21–25] is applied on PVDF; in addition, the effects of crystallinity will be incorporated. The procedure followed in the present study is based on the mechanical characterization of PVDF with different thermal histories, complemented by the characterization of the microstructure through X-ray analyses.

2 | EXPERIMENTAL

2.1 | Material preparation

PVDF (Solef®) was kindly provided by Solvay Specialty Polymers (Bollate, Italy) in form of pellets. Several plates, 0.5 and 6 mm thick, were prepared by compression molding: in all cases, the polymer pellets were put in the mold and heated up to 200°C, kept at this temperature for 15 min after which different cooling protocols were applied: slow cooling (the mold was kept in the press but the heating source was switched off), controlled cooling at a rate of 10°C/min and isothermal crystallizations at different temperatures. A summary is provided in Table 1.

2.2 | X-rays analysis

From each plate, a small sample (roughly 2 × 2 cm^2) was cut to be analyzed with wide angle X-ray diffraction (WAXD). Experiments were performed in transmission mode on a Bruker Discover D8 system equipped with a Cu-tube and Montel primary optics to provide a highly parallel beam of 0.2 mm in diameter. The Eiger2R-500 K 2D detector was installed at approximately 35 mm from the sample and images were acquired for 300 s. The background was subtracted from the obtained patterns, which were then radially integrated to obtain the intensity

TABLE 1 Cooling protocols applied

Cooling protocol	Thickness (mm)	Type of specimen	Short name
Slow cooling	0.5	Tensile, Creep	SC
10°C/min	0.5	Tensile, Creep	CC0.5
10°C/min	6	Tensile, Compression	CC6
Isoth. cryst. at 20°C	0.5	Tensile, Creep	IC20
Isoth. cryst. at 40°C	0.5	Tensile	IC40
Isoth. cryst. at 60°C	0.5	Tensile	IC60
Isoth. cryst. at 100°C	0.5	Tensile	IC100

versus scattering angle 2θ. These integrated patterns were used to obtain the weight fraction of crystallinity as

$$\chi_c = (A_{tot} - A_a)/A_{tot}, \quad (1)$$

where A_{tot} is the total intensity underneath the curve and A_a is the area underneath an amorphous halo. This amorphous halo was measured by installing a Linkam THMS600 thermal stage in the X-ray system and heating the PVDF sample (wrapped in Kapton foil) to the molten state at $T = 200$°C. Appropriate corrections for thermal expansion were taken by shifting the acquired pattern along the 2θ axis. The intensity of the halo was scaled as to match the pattern in the region between the two main crystal diffraction peaks, as shown in Figure 2.

The values obtained for the different processing conditions are included in Figure 2. Even if the adopted cooling protocols span a range of nominal cooling rates that is quite large (0.1–100°C/min), it can be observed that the degree of crystallinity does not vary strongly.

2.3 | Mechanical testing

Compression specimens of ⌀4 × 4 mm were prepared from the 6 mm thick plate (Table 1), which was first machined down to a uniform thickness of 4 mm.

Uniaxial compression tests were performed on a Zwick 1473 universal tester, equipped with a 100 kN load cell and a temperature chamber. Tests were carried out at constant true strain rates varying from 3×10^{-6} to 10^{-1} s^{-1} at temperatures of 23, 55, and 75°C. True stresses were calculated assuming incompressibility. In all cases, PTFE spray was used to lubricate the compression plates in order to avoid friction and barreling of the specimen.

Tensile specimens with a nominal cross-section of 5×0.5 mm^2, according to ISO527-1BA and a nominal cross-section of 5×4 mm^2 were cut from the plates prepared with the different cooling conditions listed in Table 1.

Uniaxial tensile tests were carried out on a Zwick Z010 universal tester, equipped with a 1 kN load cell and a temperature chamber. Tests were performed at constant strain rates varying from 10^{-6} to 10^{-1} s^{-1} and at temperatures of −10, 23, 55, and 75°C.

In each case, the yield stress σ_y was taken as the maximum stress when a clear peak could be discerned or as the intersection of the tangents to the stress–strain curve in the pre- and post-yield regions respectively.

Creep tests were performed at different constant applied stress levels and at temperatures of −10, 23, 55, and 75°C. The same specimens as for the tensile tests were used. In all cases, the target applied stress level was reached in 10 s and then kept constant until failure.

Specimens were left in the temperature chamber for 5 min in order to reach thermal equilibrium, when the test temperature was different from room temperature. Aging effects in the material were not considered in the present work; however, all the experiments were carried out in a short time frame (less than 1 week) after material preparation. Some preliminary tests revealed that no variation of properties was observed within that period of time.

3 | RESULTS

Figure 3 shows the experimental stress–strain curves, obtained at different rates and temperatures, in both tension and compression. The yield stress was found to be increasing with strain rate and decreasing with temperature, as expected. It can also be observed that the curves are less spaced for increasing temperatures, indicating that the dependence of the stress on the strain rate is less pronounced. This is even more clear if we plot the yield stress as a function of the strain rate for the different testing temperatures, see Figure 4. The yield stress strongly depends on temperature and displays a linear trend with the logarithm of strain rate. At higher temperatures and/or lower strain rates the linear trend shows a change in slope. Such response is generally interpreted as the result of a combination of different mechanisms: on one hand, at lower strain rates and high temperatures the yield kinetics are dominated by an intralamellar process

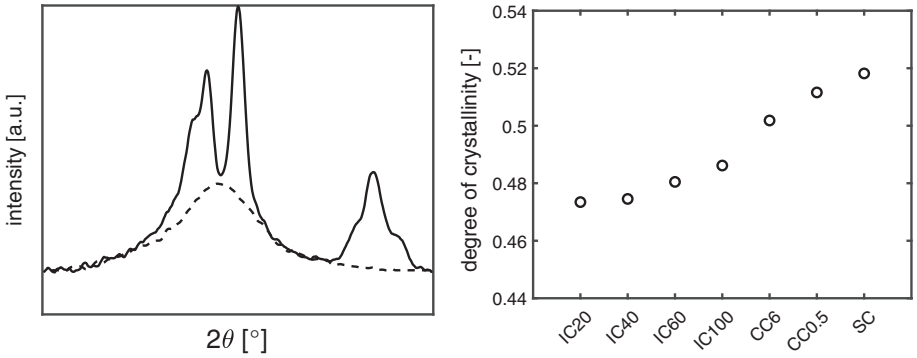

FIGURE 2 (left) wide angle X-ray diffraction radial intensity for polyvinylidene fluoride (PVDF) SC (please refer to Table 1) and (right) degree of crystallinity, χ_c, of PVDF for the different cooling protocols listed in Table 1

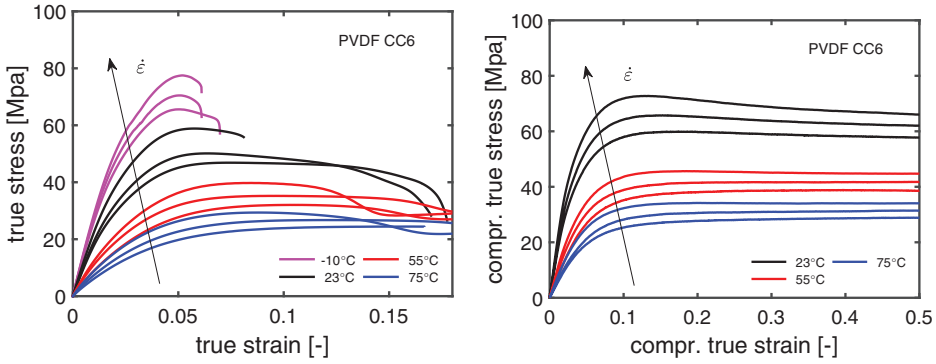

FIGURE 3 True stress versus true strain curves of polyvinylidene fluoride CC6 (please refer to Table 1) for tensile (left) and compression (right) tests at different strain rates and temperatures [Color figure can be viewed at wileyonlinelibrary.com]

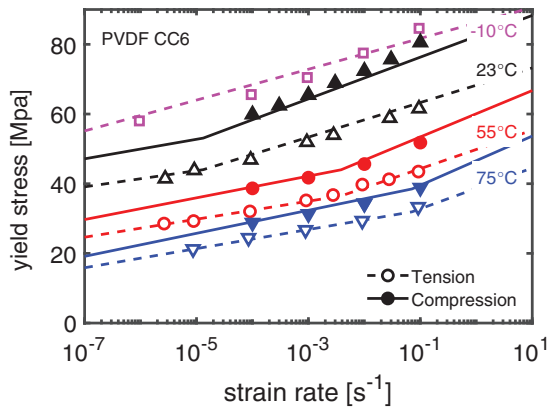

FIGURE 4 Yield kinetics of polyvinylidene fluoride CC6 (please refer to Table 1). Open and solid symbols represent experimental tensile and compressive data, respectively. Lines (solid for compression, dashed for tension) are fits obtained using Equation (7) with the parameters from Table 2 [Color figure can be viewed at wileyonlinelibrary.com]

in the crystalline phase. On the other hand, at higher strain rates and low temperatures, a second process driven by interlamellar deformation becomes active and acts in parallel to the first, resulting in a higher slope.

To describe the deformation kinetics in different loading conditions we can make use of Eyring's stress-activated flow theory[26] and the successive pressure-modified Eyring equation[27]:

$$\dot{\bar{\varepsilon}}_{pl}(\bar{\sigma},T,p)=\dot{\varepsilon}_0\sinh\left(\frac{\bar{\sigma}V^*}{kT}\right)\exp\left(\frac{\Delta H}{RT}\right)\exp\left(-\frac{\mu pV^*}{kT}\right), \quad (2)$$

where k and R are the Boltzmann's and gas constants, $\dot{\bar{\varepsilon}}_{pl}$ is the equivalent plastic flow rate, $\bar{\sigma}$ is the equivalent von Mises stress and p is the total hydrostatic pressure. $\dot{\varepsilon}_0$ is the rate factor, which depends on the thermodynamic state of the material.[28] V^* is the activation volume which describes the stress dependency, ΔH is the activation enthalpy, which takes into account the temperature dependency and μ is pressure dependence parameter, which captures the effect of hydrostatic pressure. The total hydrostatic pressure is given by

$$p=p_{atm}-\frac{1}{3}tr(\boldsymbol{\sigma}), \quad (3)$$

which in the uniaxial case becomes

$$p=p_{atm}+\alpha\bar{\sigma}, \quad (4)$$

where α depends on the loading conditions and it is equal to $-1/3$ for tension and $1/3$ for compression. Since the atmospheric pressure, p_{atm}, is in the order of 10^{-1} MPa, it can be neglected considering the order of the stresses involved.

The pressure dependence parameter can be obtained by measuring the yield stress under different

superimposed external pressures[29–31]; an alternative solution, adopted in the present work, is to combine tests in different configurations. For example, considering that in uniaxial tension and uniaxial compression the equivalent stress and the equivalent strain rate are the same (in particular they are equal to the stress σ and the strain rate $\dot{\varepsilon}$ respectively), the difference of hydrostatic stress due to the value of α in Equation (4) can be used to evaluate μ. Obviously, this only holds when the thermodynamic state of the material is the same for both loading conditions.

Given the presence of two different mechanisms, the modified equation introduced by Ree and Eyring[32,33] must be adopted. Under the assumption that different molecular processes act in parallel and that the stresses are additive, the total equivalent stress can be described as

$$\bar{\sigma}\left(\dot{\bar{\varepsilon}}_{pl},T\right)=\sum_{i=I,II}\frac{kT}{V_i^*}\sinh^{-1}\left(\frac{\dot{\bar{\varepsilon}}_{pl}}{\dot{\varepsilon}_{0,i}}\right)\exp\left(\frac{\Delta H_i}{RT}\right)\exp\left(\frac{\mu p V_i^*}{kT}\right), \tag{5}$$

in which a different set of Eyring equation parameters for each process applies. If we combine Equations (5) and (4) and we adopt the approximation $\sinh^{-1}(x)\approx\ln(2x)$, we can write

$$\bar{\sigma}\left(\dot{\bar{\varepsilon}}_{pl},T,\alpha\right)=\sum_{i=I,II}\left[\frac{kT}{(1-\mu\alpha)V_i^*}\left(\ln\left(\frac{2\dot{\bar{\varepsilon}}_{pl}}{\dot{\varepsilon}_{0,i}}\right)+\frac{\Delta H_i}{RT}\right)\right]. \tag{6}$$

Using the expression for the equivalent stress and strain rate for tension and compression, and considering them at the steady-state found at yield, for which the plastic flow rate matches the external strain rate ($\sigma=\sigma_y$, $\dot{\varepsilon}_{pl}=\dot{\varepsilon}$), we obtain the following expression for the yield stress:

$$\sigma_y(\dot{\varepsilon},T,\alpha)=\sum_{i=I,II}\left[\frac{kT}{(1-\mu\alpha)V_i^*}\left(\ln\left(\frac{2\dot{\varepsilon}}{\dot{\varepsilon}_{0,i}}\right)+\frac{\Delta H_i}{RT}\right)\right]. \tag{7}$$

The fitting lines in Figure 4 were produced with Equation (7) and the parameters reported in Table 2. An adequate agreement was found. The results for strain rates higher than 10^{-2} s^{-1} and temperatures lower than 23°C suggest the presence of a third process, as reported by Hellinckx and Bauwens.[19] However, the present data are too incomplete to fully characterize this process.

TABLE 2 Pressure modified Ree–Eyring parameters for polyvinylidene fluoride CC6

	V^* (m^3)	ΔH (J/mol)	$\dot{\varepsilon}_0$ (s^{-1})	μ (–)
Process I	3.7×10^{-27}	4.1×10^{5}	7.9×10^{48}	0.28
Process II	3.2×10^{-27}	1.4×10^{5}	8.3×10^{19}	

The parameters, used for the identification in Figure 4, are listed in Table 2. It should be noted that the rate factors, $\dot{\varepsilon}_{0,i}$, are dependent on the thermodynamic state of the material, so the values found are representative for the specific thermomechanical history of the specimens adopted to produce the results of Figure 4. On the other hand, the activation volumes, the activation enthalpies and the pressure dependence parameter are usually not influenced by the thermodynamic state.

In order to verify this hypothesis, the other processing conditions listed in Table 1 were investigated as well, following the same procedure as for the cooling protocol labeled CC6 (Figures 3 and 4). However, in this case only tensile tests were carried out.

Yield stress versus strain rate values at different temperatures are shown in Figure 5 for the different processing conditions. Experimental results were fitted again with Equation (7): apart from the rate factors, $\dot{\varepsilon}_{0,i}$, which are specific to each processing condition, all the other parameters present in Equation (7) are known. In fact, the activation volumes, the activation enthalpies and the pressure dependence parameter were kept constant and equal to the values reported in Table 2. A fitting procedure was implemented to find the alternative values of the rate factors, $\dot{\varepsilon}_{0,i}$, for each processing condition. The complete list of the parameters used to produce the curves of Figure 5 is reported in Table 3.

It can be observed from Figure 5 that for all the processing conditions a good agreement between experimental data and the pressure modified Ree–Eyring flow rule was found, thus confirming that the thermodynamic state of the material only affects the rate factors and not the other material parameters.

As proposed previously for another semi-crystalline polymer (PE),[21] a relationship between the rate factors of the Ree–Eyring model and the degree of crystallinity was investigated. Figure 6 shows the rate factors from Table 3 as a function of the values of the degree of crystallinity χ_c from Figure 2. It can be observed that, for both processes, the logarithm of the rate factors show a linear dependence on the degree of crystallinity, at least in the range investigated. Note that a decrease of the rate factors entails an increase of the yield stress, see Equation (2). Therefore, for given conditions of strain rate and temperature, an increase of the degree of crystallinity also implies increase of the yield stress. The results from Figure 6 were fitted with the following equation:

$$\dot{\varepsilon}_{0,i}=A_i\exp(B_i\chi_c). \tag{8}$$

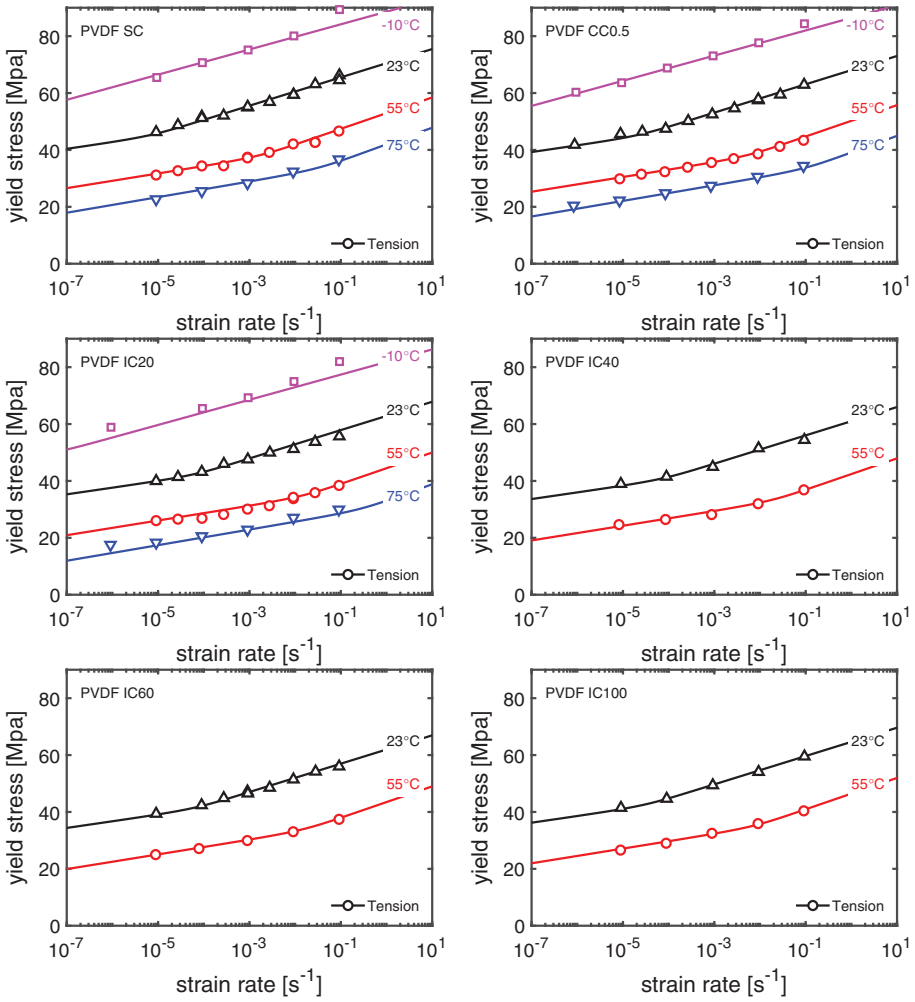

FIGURE 5 Yield kinetics of polyvinylidene fluoride prepared with different cooling protocols (please refer to Table 1). Open symbols represent experimental tensile data. Solid lines are fits obtained using Equation (7) with the parameters listed in Table 3 [Color figure can be viewed at wileyonlinelibrary.com]

TABLE 3 Pressure modified Ree–Eyring parameters for polyvinylidene fluoride for different processing conditions

	$\dot{\varepsilon}_0$ (s^{-1})		V^* (m^3)		ΔH (J/mol)		
Short name	**I**	**II**	**I**	**II**	**I**	**II**	μ (–)
SC	1.4×10^{48}	3.2×10^{19}	3.7×10^{-27}	3.2×10^{-27}	4.1×10^{5}	1.4×10^{5}	0.28
CC0.5	4.2×10^{48}	1.0×10^{20}					
CC6	7.9×10^{48}	8.3×10^{19}					
IC100	8.3×10^{49}	1.4×10^{20}					
IC60	5.1×10^{50}	2.9×10^{20}					
IC40	1.1×10^{51}	3.5×10^{20}					
IC20	2.1×10^{50}	3.0×10^{20}					

The values found for A_i and B_i are reported in Table 4.

Substitution of (8) into (7) leads to

$$\sigma(\dot{\varepsilon}, T, \chi_c, \alpha) = \sum_{i=I,II} \left[\frac{kT}{(1-\mu\alpha)V_i^*} \left(\ln\left(\frac{2\dot{\varepsilon}}{A_i \exp(B_i \chi_c)} \right) + \frac{\Delta H_i}{RT} \right) \right]. \quad (9)$$

With Equation (9) and the parameters from Table 4 the yield stress for any configuration and for any given combination of strain rate, temperature, and pressure can be predicted. It suffices to know the degree of crystallinity of the particular material under investigation. The importance and the validity of this expression will be discussed in the next section.

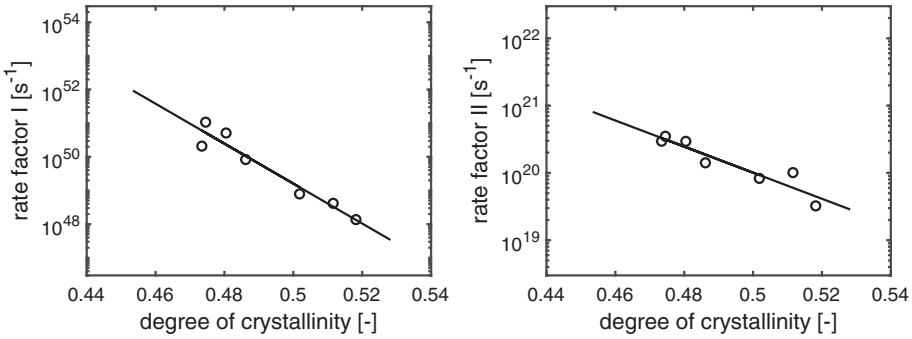

FIGURE 6 Ree–Eyring rate factors, $\dot{\varepsilon}_{0,i}$, versus degree of crystallinity, χ_c. Open symbols represent data from Table 3 and Figure 2. Solid lines are fits obtained using Equation (8) with the parameters listed in Table 4

TABLE 4 Pressure modified Ree–Eyring parameters for polyvinylidene fluoride

	V^* (m^3)	ΔH (J/mol)	A (s^{-1})	B (–)	μ (–)	c_1 (–)	c_2 (°C^{-1})
Process I	3.7×10^{-27}	4.1×10^{5}	7.4×10^{78}	−136.6	0.28	3.3×10^{-2}	1.1×10^{-3}
Process II	3.2×10^{-27}	1.4×10^{5}	5.0×10^{29}	−44.6			

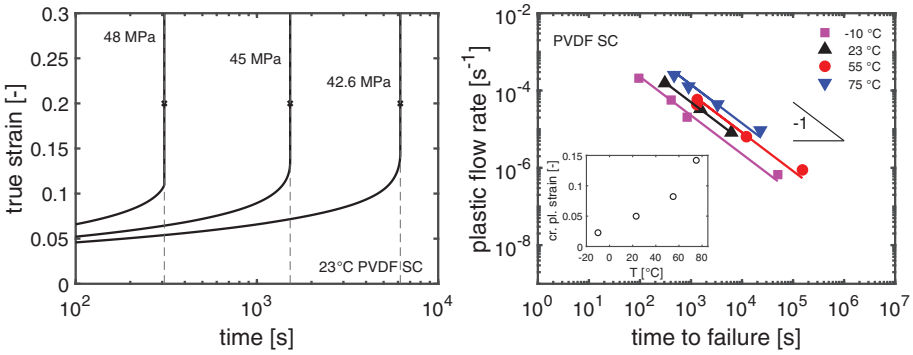

FIGURE 7 Polyvinylidene fluoride SC (please refer to Table 1): (left) strain versus time curves at 23°C. Dashed lines indicate the time to failure, t_f, for the different applied stresses. (right) plastic flow rate, $\dot{\varepsilon}_{pl}$, versus time to failure, t_f. Symbols represent experimental data, solid lines are fits obtained using Equation (10) [Color figure can be viewed at wileyonlinelibrary.com]

Figure 7 shows an example of the strain evolution in time during creep tests carried out at different levels of applied load. The time to failure, t_f, is the time at which strain localization and softening occur. During this phase, the evolution of the strain in time is very fast. As a result, the time to failure is approximately taken as the time at which a certain threshold of strain is reached (i.e., $\varepsilon = 0.2$ in Figure 7). The plastic flow rate, $\dot{\varepsilon}_{pl}$, the rate at which the strain changes in time during secondary creep, was evaluated as the minimum in the Sherby–Dorn ($\dot{\varepsilon}_{pl}$ vs. ε) curves.[34] For lifetime predictions, we make use of the concept of the critical plastic strain ε_{cr}. Assuming that the plastic flow rate induced by the applied stress entails an accumulation of plastic strain, failure is triggered once a certain critical threshold is attained.[16,35] The critical plastic strain is the amount of plastic strain that would be accumulated if the material would display plastic flow at a rate equal to $\dot{\varepsilon}_{pl}$ for its entire lifetime (t_f). It can be observed from Figures 7 and 8 that, on a double logarithmic scale, $\dot{\varepsilon}_{pl}$ and t_f show a linear relation with a slope equal to −1. Hence, results were fitted with the following expression

$$\dot{\varepsilon}_{pl}(T,\sigma)\cdot t_f(T,\sigma) = \varepsilon_{cr}(T). \tag{10}$$

The values of the critical plastic strain obtained at different temperatures for the different processing conditions are shown in Figure 9, where a clear effect of the temperature can be discerned. On the other hand, an effect of the thermodynamic state cannot be confirmed from the present results. Hence, only the dependence on temperature is taken into account, by adopting a simple linear relationship

$$\varepsilon_{cr}(T) = c_1 + c_2 T, \tag{11}$$

in order to obtain a general expression for the critical plastic strain valid for any temperature (at least in the range investigated). The values of c_1 and c_2 are reported in Table 4 with the other material parameters.

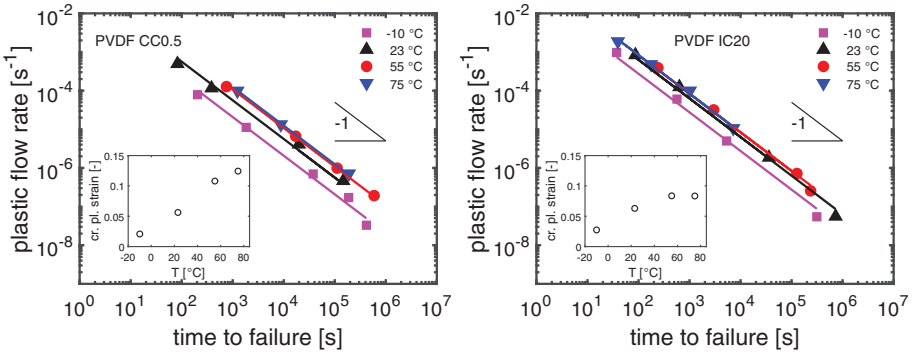

FIGURE 8 Polyvinylidene fluoride (PVDF) CC0.5 (left) and PVDF IC20 (right) (please refer to Table 1): plastic flow rate, $\dot{\varepsilon}_{pl}$, versus time to failure, t_f. Symbols represent experimental data, solid lines are fits obtained using Equation (10) [Color figure can be viewed at wileyonlinelibrary.com]

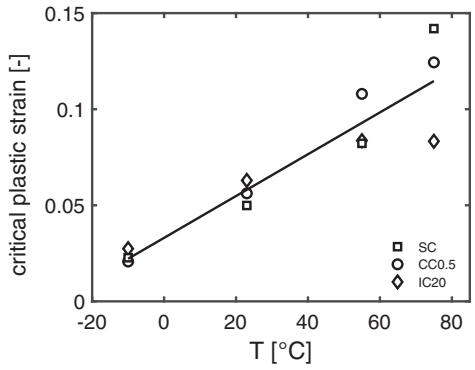

FIGURE 9 Critical plastic strain, ε_{cr}, versus temperature, T. Open symbols represent values evaluated with Equation (10); the solid line is a fit obtained using Equation (11) with the parameters from Table 4

4 | VALIDATION AND DISCUSSION

In order to investigate the validity of the model proposed, the data from Figure 5 is incorporated in Figure 10, along with the results of creep tests where available. The experimental data used to identify the rate factors in Table 3, is now plotted along with the prediction lines obtained with Equation (9) and the parameters from Table 4. It can be observed that in most cases a good agreement was found; obviously, the closer the values of the rate factors to those fitted with Equation (8) the better the agreement in Figure 10.

Equation (8) can also be used to predict the time to failure under an applied load. By combining Equations (10) and (11) and considering the equivalence between the steady state reached at yield under constant stress or constant strain rate,[20] the following relationship for the strain rate is obtained

$$\dot{\varepsilon} = \dot{\varepsilon}_{pl} = \frac{\varepsilon_{cr}}{t_f} = \frac{c_1 + c_2 T}{t_f}, \tag{12}$$

which substituted into Equation (9) leads to

$$\sigma(t_f, T, \chi_c, \alpha) = \sum_{i=I,II} \left[\frac{kT}{(1-\mu\alpha)V_i^*} \left(\ln\left(\frac{2(c_1 + c_2 T)}{t_f A_i \exp(B_i \chi_c)} \right) + \frac{\Delta H_i}{RT} \right) \right]. \tag{13}$$

Similarly to Equation (9), Equation (13) can be used to predict the stress belonging to a certain time to failure for any configuration and for any temperature provided that the degree of crystallinity is known. As Equation (13) cannot be inverted, it is not possible to evaluate the time to failure as a function of the applied stress. However, feeding a range of values of time to it, it is possible to obtain the predictions numerically. An example is shown in Figure 11, where the experimental data from creep tests are compared with the prediction lines obtained using Equation (13) with the parameters from Table 4. An excellent agreement is found for all the conditions investigated.

In order to further verify the validity of this approach, it was decided to prepare two new sets of specimens, applying different cooling protocols with respect to those already studied: an isothermal crystallization at 120°C (short name "IC120") and a quenching in salted water and ice (short name "QUE"). The testing protocol was the same as for the other processing conditions: crystallinity was measured with WAXD, creep and tensile tests were carried out at various applied stresses and strain rates respectively, but only at the temperatures of 23 and 55°C. The degree of crystallinity of the new two sets of samples is briefly reported in Table 5. The lines predicted with Equation (9) and the parameters from Table 4 are shown in Figure 12, along with the experimental yield stress values as a function of strain rate and temperature. On the other hand, Figure 13 shows the experimental creep data along with the prediction lines obtained with the parameters from Table 4 and Equation (13). Again, also for these two new processing conditions a very good agreement was found.

The results confirm the validity of the approach proposed to predict the yield kinetics directly from the degree of crystallinity of the material. The modification

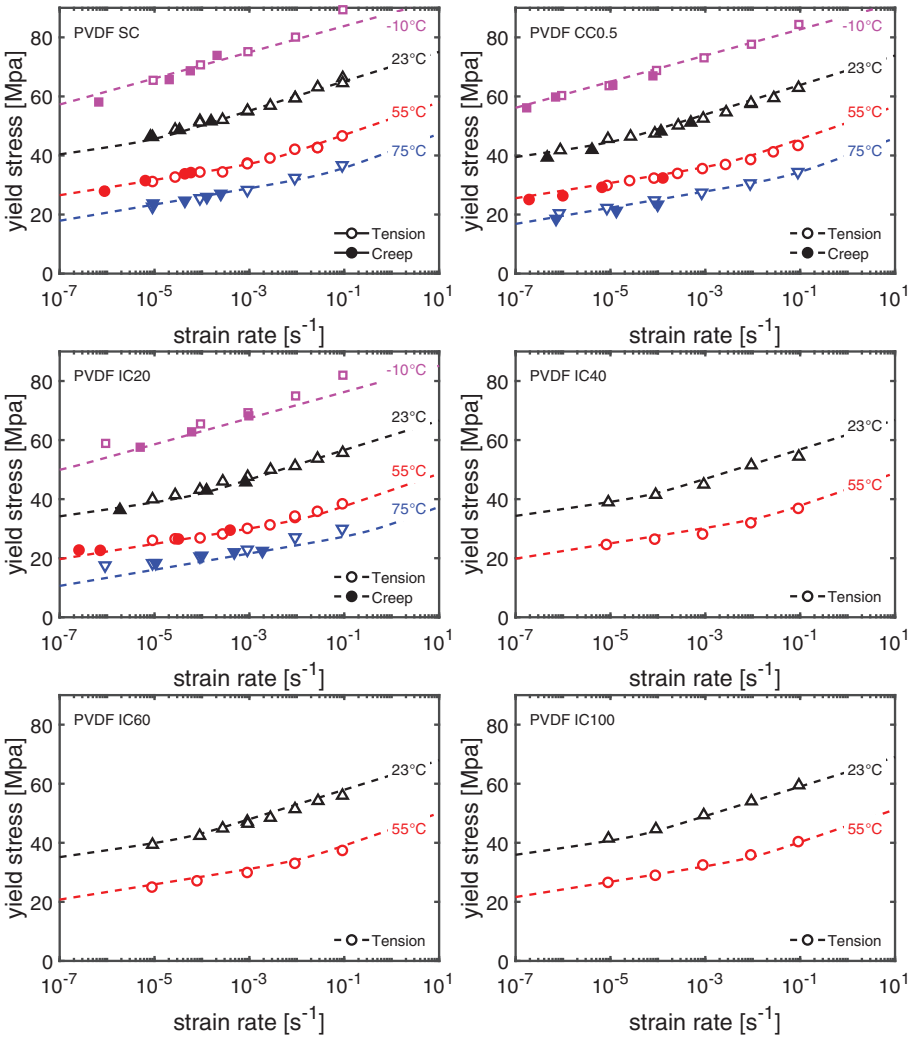

FIGURE 10 Yield kinetics of polyvinylidene fluoride prepared with different cooling protocols (please refer to Table 1). Open and solid symbols represent experimental tensile and creep data, respectively. Dashed lines are obtained using Equation (9) with the parameters from Table 4 [Color figure can be viewed at wileyonlinelibrary.com]

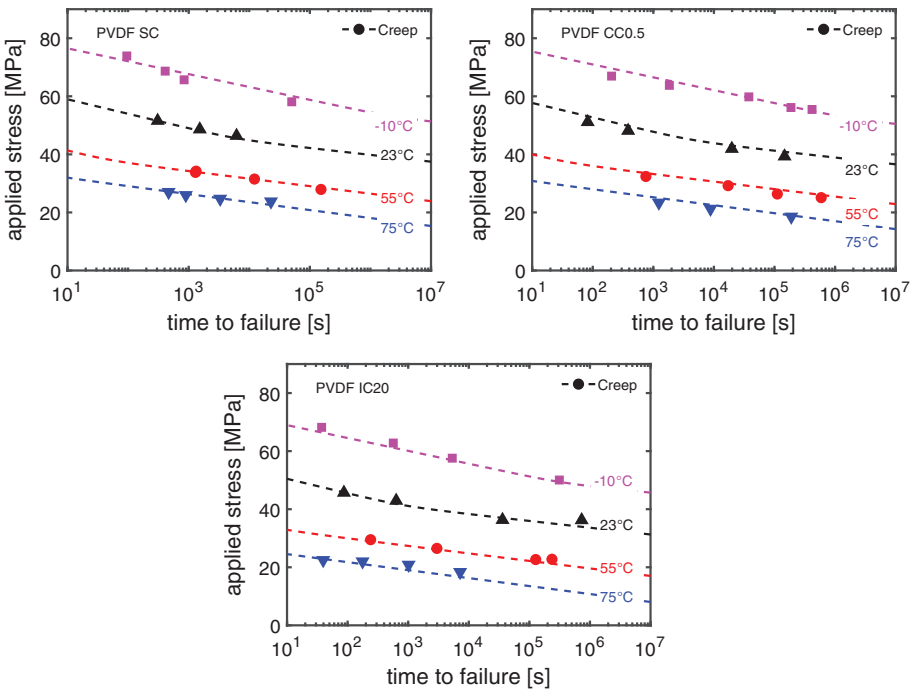

FIGURE 11 Time to failure of polyvinylidene fluoride prepared with different cooling protocols (please refer to Table 1). Solid symbols represent experimental creep data. Dashed lines are predictions obtained using Equation (13) with the parameters from Table 4 [Color figure can be viewed at wileyonlinelibrary.com]

Cooling protocol	Thickness (mm)	Type of specimens	Short name	χ_c (−)
Isoth. cryst. at 120°C	0.5	Tensile	IC120	0.493
Quenching	0.5	Tensile	QUE	0.444

TABLE 5 Additional cooling protocols applied for the validation, see also Table 1

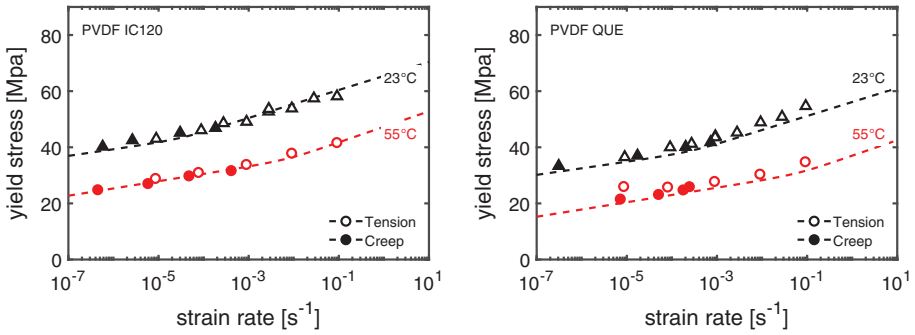

FIGURE 12 Yield kinetics of polyvinylidene fluoride prepared with different cooling protocols (please refer to Table 5). Open and solid symbols represent experimental tensile and creep data, respectively. Dashed lines are obtained using Equation (9) with the parameters from Table 4 [Color figure can be viewed at wileyonlinelibrary.com]

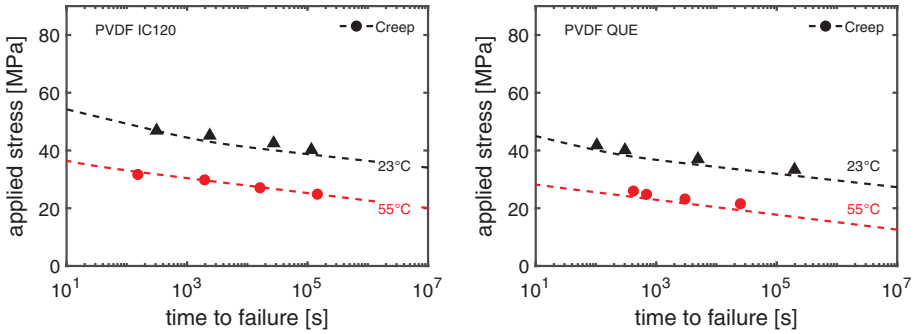

FIGURE 13 Time to failure of polyvinylidene fluoride prepared with different cooling protocols (please refer to Table 5). Solid symbols represent experimental creep data, respectively. Dashed lines are predictions obtained using Equation (13) with the parameters from Table 4 [Color figure can be viewed at wileyonlinelibrary.com]

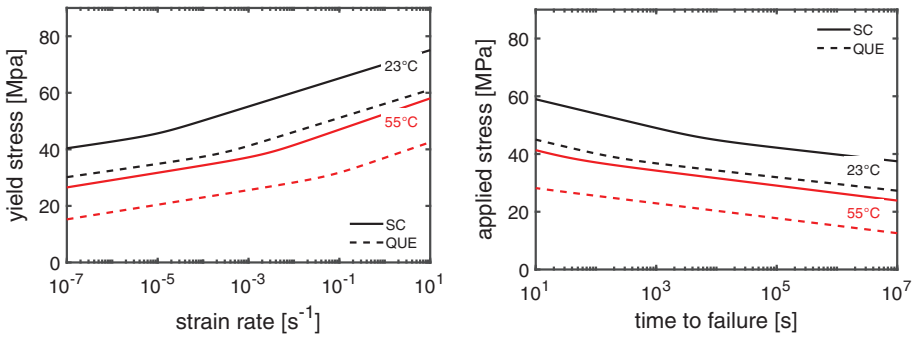

FIGURE 14 Yield kinetics (left) and time to failure (right) of polyvinylidene fluoride SC and QUE (please refer to Tables 1 and 5). Lines are obtained using Equations (9) and (13) with the parameters from Table 4 [Color figure can be viewed at wileyonlinelibrary.com]

of the Ree–Eyring flow rule introduced in Equation (9) or similarly in Equation (13) is very simple, yet very effective. In many cases the thermodynamic state of the material may be unknown for a variety of reasons. For example, processing conditions can be deliberately changed, the micro-structure of the material can be affected by fluctuations of the processing parameters or the complete thermal history is not known. Moreover, the geometry of the processed component may have a significant effect on the resulting micro-structure, even revealing spatial variations throughout the component. A measurement of the crystallinity could be sufficient to clear all these uncertainties and give a reliable prediction of the long term behavior of the material. Note that, apart from X-rays analyses, other techniques can be used to measure the degree of crystallinity as well.[36,37]

Considering all the cooling protocols applied (Tables 1 and 5), the nominal cooling rate spans a range from approximately 0.1°C/min (SC) to 100°C/s (QUE). This more or less covers the one that is typically obtained in standard processing methods for polymers and fiber reinforced composites. Hence, it is reasonable to assume that the actual manufactured components will show a degree of crystallinity, χ_c, in the range between these two extremes, that is, χ_c will vary from 0.444 to 0.518. A comparison between SC and QUE

cooling protocols can be found in Figure 14, where the yield stress versus strain curves from Figures 10 and 12 are shown together, while the prediction lines from Figure 11 are compared to those for QUE evaluated with Equation (13). Experimental results are omitted. It can be observed that, at a fixed temperature and strain rate, moving from one cooling protocol to another determines a shift in stress between approximately 8 and 12 MPa, depending if only process I or both processes are active. This indicates that even a small difference in crystallinity generates a non-negligible variation of yield stress. A similar observation can be made regarding the time to failure. Under the same conditions of applied stress and temperature, a shift between approximately 2 and 5 decades on the logarithmic time scale is obtained, depending again on how many processes are active. Obviously a shift of this extent can have a catastrophic effect if not taken into account properly. The obtained results suggest that the choice of the processing technique has a an important consequence on the time to failure: the faster the processing (i.e., higher cooling rates) the shorter the time to failure. An increased lifetime of the component may justify lower production rates.

Regardless the processing technique that is adopted, the approach proposed proved to accurately predict the long-term behavior of the material, provided that the degree of crystallinity is known.

5 | CONCLUSIONS

A large set of experiments (tension, compression, and creep) was carried out to study the yield kinetics of PVDF. We demonstrated that the yield kinetics can be modeled successfully with the pressure modified Ree–Eyring flow theory, similar to other semi-crystalline polymers. Combining the yield kinetics with the critical plastic strain concept, the time to failure in creep is accurately predicted under different combinations of applied stresses and temperature. The effect of processing conditions was taken into account by means of a simple relationship between the degree of crystallinity and the rate factors in the Eyring equation, under the assumption that the activation volumes and activation energies do not vary. The approach proposed proved to successfully predict the long-term performance of the material, regardless the processing conditions, provided that the degree of crystallinity is known.

ACKNOWLEDGMENTS

The authors would like to thank Shell Global Solutions for financial support of this study, Solvay for their kind assistance in supplying the materials and L. Pastukhov, PhD and M. Wismans, MSc for the assistance provided and for the fruitful discussions.

ORCID

Tommaso Pini https://orcid.org/0000-0002-0615-9384

REFERENCES

[1] P. Holstein, U. Scheler, R. K. Harris, *Polymer* **1998**, *39*, 4937.
[2] M. P. Silva, V. Sencadas, G. Botelho, A. V. Machado, A. G. Rolo, J. G. Rocha, S. Lanceros-Mendez, *Mater. Chem. Phys.* **2010**, *122*, 87.
[3] F. Fang, M. Z. Zhang, W. Yang, *J. Appl. Polym. Sci.* **2007**, *103*, 1786.
[4] V. Sencadas, R. Gregorio, S. Lanceros-Méndez, *J. Macromol. Sci., Part B: Phys.* **2009**, *48*, 514.
[5] H. Guo, Y. Zhang, F. Xue, Z. Cai, Y. Shang, J. Li, Y. Chen, Z. Wu, S. Jiang, *Cryst. Eng. Comm.* **2013**, *15*, 1597.
[6] J. Defebvin, S. Barrau, G. Stoclet, C. Rochas, J.-M. Lefebvre, *Polymer* **2016**, *84*, 148.
[7] B.-E. El Mohajir, N. Heymans, *Polymer* **2001**, *42*, 5661.
[8] B.-E. El Mohajir, N. Heymans, *Polymer* **2001**, *42*, 7017.
[9] M. Neidhöfer, F. Beaume, L. Ibos, A. Bernès, C. Lacabanne, *Polymer* **2004**, *45*, 1679.
[10] Y. Chen, Q.-D. Shen, W. Hu, *Polym. Int.* **2016**, *65*, 387.
[11] M. Challier, J. Besson, L. Laiarinandrasana, R. Piques, *Eng. Fract. Mech.* **2006**, *73*, 79.
[12] K. A. Esaklul, J. Mason, *Trends in Oil and Gas Corrosion Research and Technologies*, Amsterdam, The Netherlands: Elsevier BV, **2017**, p. 627.
[13] U. W. Gedde, J. Viebke, H. Leijström, M. Ifwarson, *Pol. Eng. Sci.* **1994**, *34*, 1773.
[14] R. W. Lang, A. Stern, G. Doerner, *Angew. Makromol. Chem.* **1997**, *247*, 131.
[15] H. A. Visser, T. C. Bor, M. Wolters, T. A. P. Engels, L. E. Govaert, *Macromol. Mater. Eng.* **2010**, *295*, 637.
[16] M. J. Kanters, K. Remerie, L. E. Govaert, *Polym. Eng. Sci.* **2016**, *56*, 676.
[17] A. Al-Abduljabbar, B. Melve, N. Dodds, A. Gibson, *Eng. Fail. Anal.* **2007**, *14*, 1594.
[18] A. J. de Jesus Silva, M. M. Contreras, C. R. Nascimento, M. F. da Costa, *Heliyon* **2020**, *6*, e04573.
[19] S. Hellinckx, J. C. Bauwens, *Colloid Polym. Sci.* **1995**, *273*, 219.
[20] C. Bauwens-Crowet, J. M. Ots, J. C. Bauwens, *J. Mater. Sci.* **1974**, *9*, 1197.
[21] T. B. Van Erp, D. Cavallo, G. W. Peters, L. E. Govaert, *J. Polym. Sci. Part B: Polym. Phys.* **2012**, *50*, 1438.
[22] H. Caelers, L. Govaert, G. Peters, *Polymer* **2016**, *83*, 116.
[23] E. Parodi, G. W. Peters, L. E. Govaert, *J. Appl. Polym. Sci.* **2018**, *135*, 15.
[24] F. Paolucci, G. W. M. Peters, L. E. Govaert, *J. Appl. Polym. Sci.* **2020**, *137*, 48525.
[25] L. V. Pastukhov, M. J. W. Kanters, T. A. P. Engels, L. E. Govaert, *J. Polym. Sci.* **2020**, *58*, 716.
[26] H. Eyring, *J. Chem. Phys.* **1936**, *4*, 283.
[27] I. M. Ward, *J. Mater. Sci.* **1971**, *6*, 1397.
[28] H. E. Meijer, L. E. Govaert, *Prog. Polym. Sci.* **2005**, *30*, 915.
[29] R. W. Truss, R. A. Duckett, I. M. Ward, *J. Mater. Sci.* **1984**, *19*, 413.
[30] K. Pae, *Ferroelectrics* **1984**, *57*, 249.

[31] K. Umeki, N. Takashima, T. Nakayama, N. Inoue, *Trans. Jpn. Soc. Mech. Eng. A* **1988**, *54*, 279.
[32] T. Ree, H. Eyring, *J. Appl. Phys.* **1955**, *26*, 793.
[33] T. Ree, H. Eyring, *J. Appl. Phys.* **1955**, *26*, 800.
[34] O. D. Sherby, J. E. Dorn, *J. Mech. Phys. Solids* **1958**, *6*, 145.
[35] J. M. Crissman, G. B. McKenna, *J. Polym. Sci. Part B: Polym. Phys.* **1987**, *25*, 1667.
[36] Z. Bashir, I. Al-Aloush, I. Al-Raqibah, M. Ibrahim, *Polym. Eng. Sci.* **2000**, *40*, 2442.
[37] Y. Kong, J. Hay, *Polymer* **2002**, *43*, 3873.

How to cite this article: Pini T, van Drongelen M, Remmers JJC, Geers MGD, Govaert LE. Deformation and failure kinetics of polyvinylidene fluoride: Influence of crystallinity. *J Polym Sci*. 2021;1–12. https://doi.org/10.1002/pol.20210030